2023 IEEE International Conference on Robotics and Automation (ICRA 2023)
May 29 - June 2, 2023. London, UK

Simplified Motor Primitives for Gait Symmetrization: Pilot Study with an Active Hip Orthosis

Henri Laloyaux, Chiara Livolsi, Andrea Pergolini,
Simona Crea, Nicola Vitiello, Renaud Ronsse

***Abstract*— Lower-limb exoskeletons are wearable devices whose main purposes are human rehabilitation and bilateral locomotion assistance. In particular, there is a growing interest for their use to symmetrize the gait of hemiparetic patients. This often consists in using the kinematics of the less affected side as a reference for the most affected one. In this work, we followed this approach to design a symmetrization algorithm using the formalism of motor primitives, i.e. a low-dimensional set of signals that provide the desired assistance through their combination. The amount of variables to be stored in memory is thus intrinsically limited, and this framework is particularly adapted to include other modes of assistance and/or transitions between locomotion tasks. In this paper, we report the preliminary validation of this newly developed algorithm with a hip exoskeleton and a single participant replicating hemiparetic walking. Results show that the algorithm effectively managed to reduce both temporal and spatial gait asymmetry.**

I. Introduction

Hemiparesis expresses the difficulty for someone to move half of their body and it is largely encountered in stroke survivors, due to monolateral brain damages caused by this cardiovascular accident. It is expected that 25% of people worldwide will experience a stroke once in their lifetime and their chance of survival is globally higher than 50% [1]. Approximately 80% of post-stroke patients are affected by motor impairments such as hemiparesis [2]. Among those suffering from lower limb impairments, at least a quarter will not have regained their full locomotion skills three months after the accident [3]. Despite the indisputable benefits of rehabilitation trainings, providing daily-life locomotion assistance would therefore benefit to a large population across the world.

Such assistance can be provided through leg exoskeletons, i.e. wearable robotic devices for the lower limb. Studies have already been carried out for this purpose with different robots such as rigid powered orthoses for the ankle [4], the knee [5], or two joints actuated at the same time such as knee and hip [6]. Soft exosuits have also been investigated for robot-aided training [7]. Studied populations include mainly stroke survivors but also people affected by other disorders such as spinal cord injury and Guillain-Barré syndrome [4].

Several control strategies have been developed to govern the behavior of these devices when interacting with human users [8], [9], [10]. Typically, these strategies can be sorted into two main families: (i) those aiming at delivering a given (adaptive) torque pattern to the affected joint, possibly mimicking the joint torque profile of healthy people, identified through inverse dynamic analysis; and (ii) those aiming at mirroring the impaired joint kinematics and the contralateral sound one, delivering assistance as long as these profiles differ from each other. Interestingly, both approaches led to similar results regarding locomotion recovery [5].

However, even the less affected leg of stroke survivors displays spatio-temporal gait characteristics that differ from the ones of healthy people. Consequently, this would be valuable to combine these two strategies: delivering an assistive torque profile would indeed directly benefit both sides, while adding another action to specifically symmetrize would contribute to restore a healthy spatiotemporal gait pattern. A promising formalism to combine both approaches is the one relying on motor primitives: these are simple and monotonic signals [11], which are linearly combined in order to compose complex patterns. Therefore, the same primitives could be used both to deliver stationary assistance, and adapted to reach gait symmetry, by proper tuning of their weights. Interestingly, previous research has already investigated the use of primitive-based control for providing walking assistance [12], [13]. In the present paper, we report a new algorithm leveraging this concept of primitives for gait symmetrization. In a nutshell, the kinematics of both hips are continuously measured in order to quantify their asymmetry, and the weights are adapted to minimize this difference.

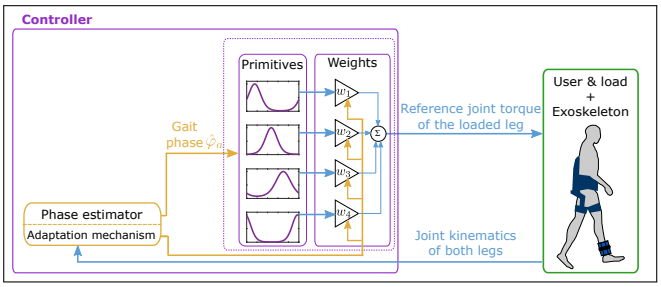

Fig. 1: General diagram of the primitive-based control strategy. The symmetrization algorithm governing phase estimation and weights adaptation is highlighted in yellow and detailed in Figure 2.

H. Laloyaux and R. Ronsse are with the Institute of Mechanics, Materials, and Civil Engineering (iMMC), the Institute of NeuroScience (IoNS) and the Louvain Bionics of UCLouvain, Louvain-la-Neuve, Belgium henri.laloyaux@uclouvain.be. C. Livolsi, A. Pergolini, S. Crea and N. Vitiello are with the BioRobotics Institute and the Department of Excellence in Robotics and AI, Scuola Superiore Sant'Anna, Pisa, Italy. S. Crea and N. Vitiello are with the Fondazione Don Gnocchi, Florence, Italy. S. Crea and N. Vitiello have commercial interests in IUVO S.r.l., the company that owns the IP rights of the APO technology.

A first pilot study of this symmetrization algorithm was carried out in this paper. A healthy subject wore a load distally on one ankle in order to reproduce a hemiparetic walk. Assistance was provided thanks to a hip exoskeleton and compared to a control condition in zero-torque mode. The asymmetry is quantified for these conditions, both spatially – i.e. by quantifying the difference between both joint angle profiles – and temporally – i.e. by analyzing the occurrence of the gait events like foot contact and toe off.

The algorithmic developments and experimental methods of this study are detailed in Section II. In Section III, the main results are presented and discussed. Finally, Section IV concludes this paper and provides insights for future works.

II. Materials and Methods

In this section, we first introduce the mathematical developments that support the orthosis control law towards walking symmetrization. Next, experimental methods of a first pilot study with this algorithm are described, along with the considered asymmetry metrics.

A. Control strategy

Figure 1 overviews the general control strategy, highlighting the newly developed adaptation mechanism in order to symmetrize the user gait. This algorithm also provides an estimation of the gait phase through dynamic filters following the methodology described in [14].

1) Primitive-based control framework: In our primitive-based formalism, a desired torque $\tau(\varphi)$ to be applied to the affected side is computed as the sum of 4 phase-dependent periodic Gaussian-shaped primitives $P_m(\varphi)$ multiplied by their weight w_m:

$$\tau(\varphi) = \sum_{m=1}^{4} w_m \, P_m(\varphi) \tag{1}$$

where φ is the phase of the gait cycle and the primitives are parametrized through their peak location φ_m and their width σ_m:

$$P_m(\varphi) = \exp\left(\frac{\cos\big(2\pi(\varphi - \varphi_m)\big) - 1}{\sigma_m}\right). \tag{2}$$

These primitives $P_m(\varphi)$ are thus equal to 1 at their peak value, occurring when the phase is equal to φ_m. They were obtained thanks to a series of heuristic and deterministic optimization [15], [16] and are shown in Figure 2. Contrarily to our previous work [16] where they were elements of virtual muscle stimulations, they serve here as direct torque compounds, following the approach called "dynamic primitives" in [12].

The primitive weights and the gait phase are computed by our new adaptation algorithm, which works in two steps. First, adaptive oscillators (AOs) continuously estimate both the phase and the difference between kinematic profiles of both hips. Then, four times per cycle – corresponding to the phase of the activation peak of the four primitives, i.e. φ_m – it updates the weights w_m in order to reduce this difference between angular profiles, and thus to increase bilateral symmetry. Figure 2 illustrates this process.

2) Estimation of the difference between angular profiles: A low-pass filtered angle profile $\hat{\theta}_s(\varphi_s)$ of the sound leg is continuously computed from the measured joint angle $\theta_s(t)$ of the same leg:

$$\hat{\theta}_s(\varphi_s) = \mathcal{A}\{\theta_s\,(t_0 \rightarrow t)\,, \varphi_s^0 := \varphi_{\max\theta_s}\} \tag{3}$$

where $\mathcal{A}$ is the dynamic filtering operation performed by AOs on the measured joint angle. The phase reset φ_s^0 of this profile is set to correspond to the phase $\varphi_{\max\theta_s}$, which is the phase of the estimated maximum hip flexion angle of this leg. This computation is detailed in Appendix A.

This process is duplicated for the affected side:

$$\hat{\theta}_a(\varphi_s) = \mathcal{A}\{\theta_a\,(t_0 \rightarrow t)\,, \varphi_s^0 := \varphi_{\max\theta_s}\}. \tag{4}$$

More details about this operation can be found in Appendix A. Note that the phase reset is again synchronized with the estimated maximum flexion of the sound hip instead of the one of the affected side, for the following reason. There is indeed an interest of using a common reference for both legs, since their gait phases are not exactly shifted by 50% in people with asymmetric gait disorders, such as post-stroke people [17]. Therefore, taking a common reference phase for both legs will contribute in reducing the temporal asymmetry between both sides, on top of spacial asymmetry.

The reference phase for the affected side is computed by shifting the one of the sound side by 50%, i.e.:

$$\hat{\varphi}_a \triangleq \mod(\varphi_s + 50\%, 100\%). \tag{5}$$

This shifted phase $\hat{\varphi}_a$ thus represents the ideal cycle phase of the affected side in case of perfect temporal symmetry.

The difference $\Delta\hat{\theta}(\hat{\varphi}_a)$ between both kinematic profiles at the same phase of their corresponding gait cycle can then be computed as:

$$\Delta\hat{\theta}(\hat{\varphi}_a) = \hat{\theta}_s(\hat{\varphi}_a) - \hat{\theta}_a(\varphi_s). \tag{6}$$

This difference thus accounts for both spacial asymmetries – captured by the parameters of the two independent filters – and temporal asymmetries – captured by forcing the phase of the affected side to be exactly in opposition with respect to the one of the sound side.

3) Adaptation of the primitive weights: During a given cycle c, when the estimated phase $\hat{\varphi}_a$ equals the peak phase φ_m of a primitive, i.e. for $m \in [1\,;\,4]$, the update process of this primitive weights is activated. At that time, a desired supplementary torque $\Delta\tau^c(\varphi_m)$ – defined positive in flexion – has to be delivered to the affected leg, in order to reduce leg asymmetry:

$$\Delta\tau^c(\varphi_m) = k_1 \, \Delta\hat{\theta}(\varphi_m) \tag{7}$$

where k_1 is a strictly positive constant with a low value to avoid adaptation overshoot. This extra torque would reduce kinematic asymmetry acting both on spatial variables – since the torque pattern is adapted as a function of the difference between kinematic profiles – and on temporal variables – since it depends of the phase of the sound leg.

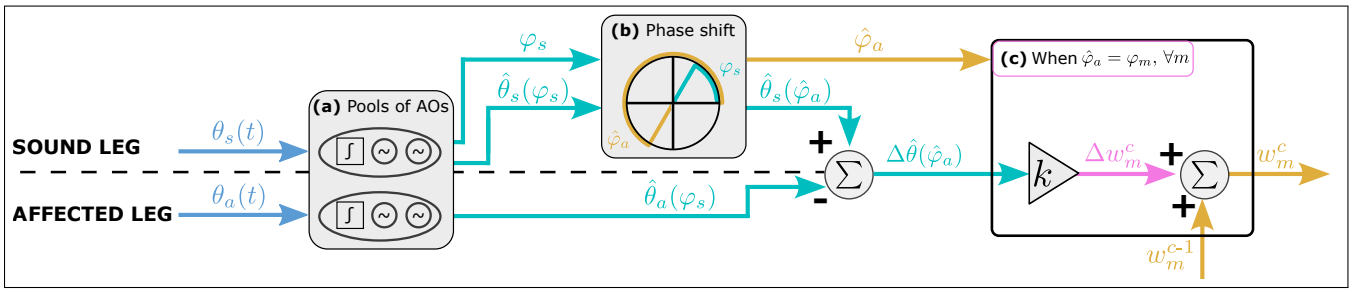

Fig. 2: Global architecture of the asymmetry reduction algorithm: (a) From both instantaneous joint kinematics $\theta_s(t)$ and $\theta_a(t)$, the main phase of the sound leg φ_s is determined by adaptive oscillators, as well as the average filtered kinematics profiles $\hat{\theta}_s(\varphi_s)$ and $\hat{\theta}_a(\varphi_s)$; (b) The kinematic profile $\hat{\theta}_s(\varphi_s)$ of the sound leg is phase-shifted by 50% in order to be aligned to the one of the affected leg. The kinematic difference between both legs $\Delta\hat{\theta}(\hat{\varphi}_a)$ is computed and used as error signal to drive the adaptation mechanism of the primitive weights; (c) When $\hat{\varphi}_a$ is equal to the peak location φ_m of a primitive m, a supplementary weight Δw_m^c is computed from $\Delta\hat{\theta}(\hat{\varphi}_a)$, and added to the previous primitive weight w_m^{c-1} to update it.

The desired supplementary torque is computed at the peaks of the primitives for the following reasons:

1) They are relatively well-distributed along the gait cycle, see Figure 1.
2) The computed supplementary torque will propagate to the whole cycle, with a decay that is governed by the shape of the primitives. It will thus never be larger than at the phase where it is computed, i.e. where the primitive reaches its maximal influence.

In order to apply this desired supplementary torque $\Delta\tau^c(\varphi_m)$, the weight associated to the corresponding primitive P_m will be updated proportionally to it:

$$\Delta\tau^c(\varphi_m) = k_2\,\Delta w_m^c. \tag{8}$$

From Equations (7) and (8), the value of this supplementary weight Δw_m^c is thus directly proportional to the kinematic difference at the primitive peak location, i.e.:

$$\Delta w_m^c = k\,\Delta\hat{\theta}(\varphi_m) \tag{9}$$

where $k = k_1/k_2$ is actually the only gain that has to be tuned in this algorithm.

The primitive weights are then updated:

$$w_m^c = w_m^{c-1} + \Delta w_m^c \tag{10}$$

where w_m^0 is set to 0 in order to be in zero-torque mode (transparent mode, TM) before the onset of the gait symmetrization process.

B. Pilot study

A healthy 28 year-old male ($1.70\,\mathrm{m}$, $68\,\mathrm{kg}$) volunteered to assess the performance of this symmetrization strategy. In order to replicate a hemiparetic walk on him without modifying its anatomy, we followed the guidelines of [18] and opted for adding a load at one of his ankles. Preliminary experiments showed that adding a supplementary weight on the non-dominant side (in this case his left leg) induced a greater asymmetry than on the dominant side [19] and that a load weight of approximately 10% of his body mass would induce hip kinematics close to the ones of post-stroke people. This was hence followed in this pilot study and is later designated as "load-asymmetrized" condition.

The study was carried out at The BioRobotics Institute of the Scuola Superiore Sant'Anna (Pontedera, Italy) in accordance with the declaration of Helsinki and the subject gave his informed consent prior to the experimentation.

1) Experimental setup: The participant was equipped with a $7.0\,\mathrm{kg}$ load made of fitness soft dumbbells on his left ankle, and wore an Active Pelvis Orthosis (APO). This is an exoskeleton conceived for assisting both hips in the sagittal plane and experimented on different user profiles such as healthy subjects [20], elderly people [21] and transfemoral amputees [22]. The first APO prototypes were developed within the CYBERLEGs research project [23], then the technology was licensed to IUVO S.r.l., a spin-off company of the same institution. Although the APO is a bilateral device, here only the loaded side (left) is assisted, the non-loaded leg (right) staying in zero-torque mode in all conditions.

Shoes with pressure-sensitive insoles were also worn to compute the vertical ground reaction force of each leg, allowing to detect HS and toe off (TO) events [24].

The software routine embedded in the APO stored the gait events detected by the sensorized insoles, as well as all the different variables mentioned in Section II-A and appendix A, from the measured joint angles of both hips $\theta_s(t)$ and $\theta_a(t)$ to the delivered torque $\tau(t)$.

2) Experimental protocol: First, the load-asymmetrized participant was asked to walk in TM on a treadmill at a self-selected speed, which was found to be $2.0\,\mathrm{km/h}$. After a rest, the proper experiment was conducted.

This experimentation consisted of a series of different conditions, starting from a transparent mode – designated here as TM#1 – where the participant walked at his preferred speed until the error signals of the AOs reached convergence.

The second experimental condition consisted in activating the symmetrization algorithm on the loaded leg, with an update gain equal to $k = 0.3\,\mathrm{Nm\,deg^{-1}}$.This is called the first symmetrization mode (SM#1) and it lasted for 35 gait cycles. A second symmetrization mode (SM#2) followed where k was doubled to $0.6\,\mathrm{Nm\,deg^{-1}}$, during a similar number of cycles. Finally, another transparent mode with a similar duration (TM#2) was performed.

3) Data processing: The kinematic and temporal variables recorded by the APO and the pressure-sensitive insoles (i.e. hip joint angles, HS and TO) were segmented based on the real HS of the non-loaded leg. Only the last 20 cycles of each of the four conditions were kept for the analyses, in order to focus the analyses reported here on steady-state behavior. These data were resampled over 100 points equally spaced across cycles, and then these time-normalized profiles were averaged.

For each condition, 4 asymmetry metrics were computed:

1) The RMS difference between the kinematic profiles:

$$\Delta_{RMS} \triangleq \mathrm{RMS}\left(\theta_s(\hat{\varphi}_a) - \theta_a(\varphi_s)\right) \; ; \qquad (11)$$

2) The Phase-shifted Relative Delay between HS:

$$\delta_{HS} \triangleq \frac{|T_{HS}^{a\to s} - T_{HS}^{s\to a}|}{T^{cycle}} \qquad (12)$$

where T^{cycle} is the total time of a gait cycle and $T_{HS}^{s\to a}$ (*resp.* $T_{HS}^{a\to s}$) is the time between the HS of the non-loaded (*resp.* loaded) leg and the HS of the other side, as illustrated in Figure 3 ;

3) Similarly, the Phase-shifted Relative Delay between TO:

$$\delta_{TO} \triangleq \frac{|T_{TO}^{a\to s} - T_{TO}^{s\to a}|}{T^{cycle}} \; ; \qquad (13)$$

4) The Rectified Overall Temporal Asymmetry:

$$\Xi_{T,Asym}^{Rec} \triangleq \max\left(\Xi_{T,Sym}, \Xi_{T,Sym}^{-1}\right) - 1 \qquad (14)$$

where $\Xi_{T,Sym}$ is the Overall Temporal Symmetry [25], i.e. a ratio of the durations of the swing and stance phases of both legs, as depicted in Figure 3:

$$\Xi_{T,Sym} = \frac{T_a^{TO\to HS}/T_a^{HS\to TO}}{T_s^{TO\to HS}/T_s^{HS\to TO}}. \qquad (15)$$

While δ_{HS} and δ_{TO} are metrics capturing the delays between gait events, $\Xi_{T,Asym}^{Rec}$ provides an insight on the symmetry of the durations of swing/stance phase.

These four custom-defined metrics capture therefore both kinematics and temporal asymmetries They are by definition restricted to be positive, with 0 corresponding to a perfectly symmetric gait.

The significance of the symmetrization in SM#1 and SM#2 was assessed by performing the Welch ANOVA test for unequal variances [26] for the four asymmetry metrics in MATLAB (R2016b, The MathWorks Inc., Natick, MA) [27]. A post-hoc Tukey-Kramer's test was later realized to pairwise compare the conditions, and differences with $p < 0.05$ were considered as being significant. Since only one participant was recruited in the preliminary experiment reported in this paper, statistics have been computed across conditions and with one value per stride. Our results should thus be handled with care in comparison to those collected with a larger population, that typically use analysis of variance across several subjects.

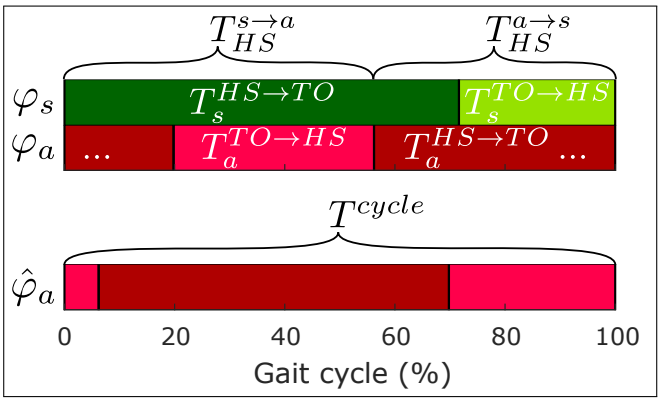

Fig. 3: Temporal events and the intermediate times. A darker (*resp.* lighter) rectangle represents the stance (*resp.* swing) phase. While the two upper cycles – φ_s and φ_a – start from the HS of the sound leg, the third one – $\hat{\varphi}_a$ – is phase-shifted by 50% to highlight the delays between gait events. The inter-TO times are not depicted here, although they can be found through the same reasoning as the inter-HS ones.

III. Results and Discussion

A. Kinematics and gait phases along the gait cycle

The mean profiles of the hip kinematics and the gait phases in TM prior to the symmetrization assistance are shown in Figure 4, left panel. This figure shows that TM#1 replicated five typical features of post-stroke gaits with a medium to fast speed (i.e. 0.41 ± 0.08 to 0.63 ± 0.08 m/s) [17], [28], i.e. that they have :

(i) a longer swing phase on their most affected leg than on the less affected one ;
(ii) their foot contact of this weakened side at around 55% of the cycle starting from the contralateral HS ;
(iii) the extension peak of their most affected side earlier in the cycle ;
(iv) their flexion peak lower on the less affected side ;
(v) less flexion on the weakened side for the first $\approx$ 25-55% of the gait cycle.

In sum, the asymmetric gait profile of a typical post-stroke walker was well replicated by the participant wearing an ankle load equal to 10% of his body mass.

Figure 4 shows that triggering the symmetrization assistance had the expected effect. In particular:

(i) Swing duration of the loaded side is shorter when assistance is on. However, it is still longer than on the non-loaded side. Noticeably, this effect persisted after the assistance was removed, i.e. in TM#2.
(ii) Phase shifts between HS on both legs were closer to the expected value shifted by 50% when assistance was switched on. Again, this effect persisted in TM#2.
(iii) The synchronization of extension peaks was improved in SM (with an average delay reduced to around 2%). Interestingly, this is the symmetrization feature that was the most clearly washed out in the TM#2 condition.
(iv) Hip flexion peak of the loaded side was more similar to the one of the other side, with assistance being

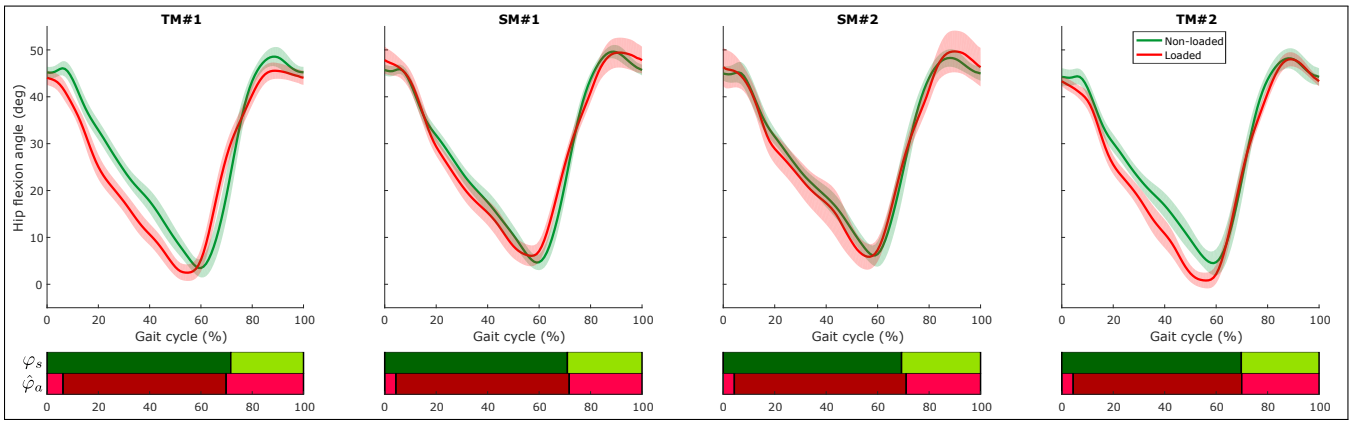

Fig. 4: Above: Hip joint kinematics along the gait cycle, averaged across the last 20 cycles of each condition. Shadowed areas capture one standard deviation. The beginning of the gait cycle is defined as the non-loaded HS (*resp.* $+50\%$) for the non-loaded (*resp.* loaded) side. Below: Mean gait phases along these cycles, using the convention displayed in Figure 3.

switched on. Interestingly, cycles displayed more variability around this phase in SM. This is possibly due to the proximity of this flexion peak and peak locations of primitives C and D, which would generate higher peak torques at this moment of the gait cycle.

(v) Both assisted conditions (SM#1 and SM#2) induced hip angular profiles being globally similar between both hips, thus achieving gait symmetrization. However, kinematic variability is about twice as high in SM#2 than in SM#1. This might reveal that the higher value of k tested in SM#2 was inducing behavioral oscillations in the human-robot interaction, and thus that lower values should be kept for safety reasons.

Finally, one can notice that the angle profile of the non-loaded side remained almost identical across conditions, which would be another desirable outcome. Indeed, [17] reported that the kinematics of the unaffected side of post-stroke patients is more similar to the ones of healthy people.

B. Asymmetry metrics

Symmetrizing effects can actually be observed for each of the four asymmetry metrics, as reported in Table I.

TABLE I: Welch-ANOVA results for the asymmetry metrics

Δ_{RMS}	δ_{HS}	δ_{TO}	$\Xi^{Rec}_{T,Asym}$
F(3,76) = 20 $p < 0.001$	F(3,76) = 8.9 $p < 0.001$	F(3,76) = 12 $p < 0.001$	F(3,76) = 11 $p < 0.001$

Moreover, as illustrated in Figure 5, significant differences were systematically present between each symmetrizing mode and TM#1. This was also the case between TM#2 and TM#1, suggesting a (partial) retention of the symmetrized behavior induced by the assistance once it was switched off However, reproducing this experiment with a larger pool of subjects and with a longer inter-recordings time would be needed to answer this question.

TM#2 displayed only one metric being significantly different to an assisted condition, namely the Δ_{RMS} metric that was significantly larger in TM#2 than in SM#1. This reinforces the assumption that the participant adopted a walking gait during TM#2 that was in-between the original one (TM#1) and the one acquired during the assisted conditions.

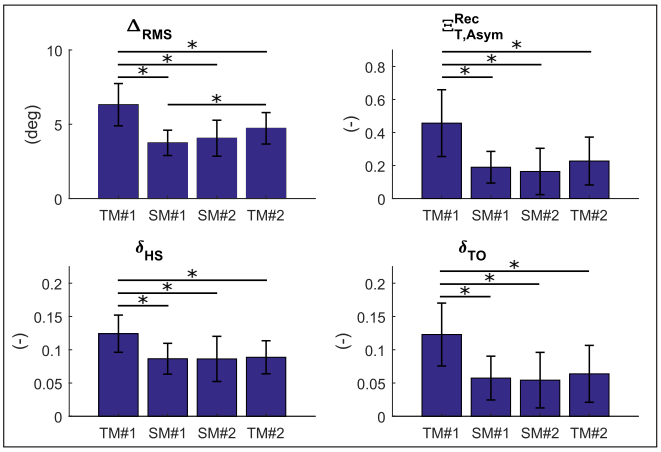

Fig. 5: Mean values and standard deviations of the four asymmetry metrics. Asterisks denote statistically-significant differences between conditions ($p < 0.05$).

IV. Conclusion and Perspectives

In this work, a symmetrization algorithm for a hip orthosis has been presented and tested in a first pilot study. This control strategy leverages adaptive oscillators and periodic Gaussian-shaped primitives. The weights associated to the latter are adapted once per cycle in order to enhance the gait symmetry. This results in an adaptive control framework with a relatively low number of parameters and variables to be stored in memory, i.e. 27 in our case: 11 for the AOs state variables, 3 for the parameters governing the AOs dynamics, 1 for the adaptation gain k, 8 for the primitives parameters and 4 for their weights.

Recently, two other symmetrization algorithms for hip exoskeletons have been published [29], [30]. Both share a key difference with our own approach, in the sense that only up two torque peaks per cycle were delivered, while this can reach four in our case. The control strategy in [29] differed also from ours since the timing and the width of the torque peaks were adapted besides their amplitude, and that a model-free reinforcement learning-based control framework was used for adapting the peaks parameters. Interestingly, the

algorithm described in [30] also relied on AOs very similar to ours. However, its parameters are updated at variable timings during the cycle, following non-linear relationships between the kinematic difference and the supplementary weights.

One healthy subject took part in this pilot study. We made him display a hemiparetic-like gait by adding a distal load on one of his ankles. This proved inducing walking characteristics similar to post-stroke patients, with a strong asymmetry between both sides. This walking asymmetry was mitigated by our assistive controller, as captured by four asymmetry metrics.

Interestingly, this overall symmetrization of the gait was not entirely washed out after switching off the assistance, showing that the assisted conditions might induce some retention. To the best of our knowledge, wash-out effects on gait asymmetry have not been studied yet with powered orthoses. In contrast, people studied wash-out dynamics with split-belt treadmill walking, and it was observed that the treadmill-induced asymmetry decreases quickly during the wash-out phase [31]. In contrast, retention is stronger when visual and auditory augmented biofeedback is provided to manipulate gait symmetry features [32]. These results have to be confirmed with a larger pool of participants. This would further allow assessing the symmetrization impact on other gait variables – such as step length and knee/ankle kinematic profiles – or on muscular activity of both legs.

A possible improvement to the designed control strategy would be a thoughtful selection of the primitives parameters: since the weights update occurs only when the primitives reach their peaks, a new primitives extraction stemming from hemiparetic patients' kinematics would probably better tailor the provided assistance.

Owing to the use of the same primitives for a walking assistance purpose [16], combining symmetrization and bilateral assistance is another perspective. Adding a bio-inspired layer simulating the hip musculoskeletal dynamics [12] is another improvement that could be envisaged towards better bio-inspiration of our algorithm.

APPENDIX

A. Estimation of the average angle profiles

AOs are dynamic filters applied to (possibly) noisy rythmic signals [33]. Phase estimation and low-pass filtering are two of their functionalities used in this work.

1) General AOs formulas: The error signal $F_s(t)$ of the kinematics reconstruction is defined at each sample t as:

$$F_s(t) \;=\; \theta_s(t) \;-\; \left(\sum_{i=1}^{N} \alpha_{s,i} \cos\left(\varphi_{s,i}(t)\right) + \alpha_{s,0} \right). \quad (16)$$

Here, the number of AOs was set to $N = 2$ due to the fact that typical hip angular profiles are quasi-sinusoidal.

State variables of $F_s(t)$ are computed following [14]. These equations are however modified in order to have the phase reset of the learned signal $\theta_s(t)$ when it reaches its maximum value, i.e. :

$$\dot{\varphi}_{s,i}(t) = \omega\, i - \nu_\varphi \frac{F_s(t)}{\sum_{j=1}^{2} \alpha_{s,j}} \sin\left(\varphi_{s,i}(t)\right), \quad (17)$$

$$\dot{\alpha}_{s,i}(t) = \eta\, F_s(t) \cos\left(\varphi_{s,i}(t)\right), \quad (18)$$

$$\dot{\alpha}_{s,0}(t) = \eta\, F_s(t) \quad (19)$$

where ν_φ and η are constant strictly positive gains. The frequency ω is governed as follows:

$$\dot{\omega}(t) = \frac{-\nu_\omega}{2} \left(\frac{F_s(t) \sin\left(\varphi_{s,1}(t)\right)}{\sum_{j=1}^{2} \alpha_{s,j}} + \frac{F_a(t) \sin\left(\varphi_{a,1}\right)}{\sum_{j=1}^{2} \alpha_{a,j}} \right)$$

where $F_a(t)$, $\alpha_{a,j}$ and $\varphi_{a,1}(t)$ are the equivalent state variables of the affected side and ν_ω is another positive gain.

Parameters η, ν_ϕ and ν_ω were respectively set to $0.5\ \mathrm{s}^{-1}$, $5.5\ \mathrm{rad/s}$ and $1.25\ \mathrm{rad/s}^2$ in order to have learning time constants of $4\ \mathrm{s}$ [33]. This time was chosen because it corresponds approximately to the interval of a U-turn for a healthy walker, thus limiting the transient effects should this algorithm be later used in an ecological context.

2) Reformulation for a unique gait phase: A change of variables can be performed to express the phase of each AO $\varphi_{s,i}$ according to the main phase $\varphi_{s,1}$. Assuming at a given time that the state variables ω, $\alpha_{s,i}$ and $\alpha_{s,0}$ will stay constant in the near future, $F_s(t)$ becomes null from Equation (19) and Equation (17) simplifies in:

$$\dot{\varphi}_{s,i} = \omega\, i. \quad (20)$$

For each AO i, its phase shift towards the first AO can be defined as:

$$\varphi^0_{s,i} \triangleq \varphi_{s,i} - i\, \varphi_{s,1} \quad (21)$$

and it will stay constant from Equation (20).

Therefore, the phase of this AO i can be rewritten as:

$$\varphi_{s,i} = i\, \varphi_s + \varphi^0_{s,i} \quad (22)$$

where $\varphi_s \triangleq \varphi_{s,1}$.

The reconstructed angle profile can then be expressed as:

$$\hat{\theta}_s(\varphi_s) = \sum_{i=1}^{2} \alpha_{s,i} \cos\left(i\, \varphi_s + \varphi^0_{s,i}\right) + \alpha_{s,0}. \quad (23)$$

By making the hypothesis that $\theta_s(\varphi_s)$ and $\hat{\theta}_s(\varphi_s)$ have their maximum at the same gait phase, $\varphi_{\max \theta_s}$ is thus defined as the phase where $\hat{\theta}_s(\varphi_s)$ reaches its maximum. Pilot studies showed that $\alpha_{s,2} \ll \alpha_{s,1}$ and thus $\hat{\theta}_s(\varphi_s) \approx \alpha_{s,1} \cos\left(\varphi_s\right) + \alpha_{s,0}$, which reaches its highest value when $\varphi_s = 0$. Hence, $\varphi_{\max \theta_s}$ is simply set to 0 here.

For the other leg, Equations (16) to (20) are adapted identically to the affected joint angular profile. Similarly, each AO phase $\varphi_{a,i}$ can be expressed according to the main phase φ_s of the sound leg:

$$\varphi_{a,i} = i\, \varphi_s + \varphi^0_{a,i} \quad (24)$$

where $\varphi^0_{a,i}$ is its phase shift towards the main phase φ_s of the sound leg and should stay constant.

The reconstructed joint angle profile is then expressed as:

$$\hat{\theta}_a(\varphi_s) = \sum_{i=1}^{2} \alpha_{a,i} \cos\left(i\, \varphi_s + \varphi^0_{a,i}\right) + \alpha_{a,0}. \quad (25)$$

REFERENCES

[1] V. L. Feigin *et al.*, "World stroke organization (wso): global stroke fact sheet 2022," *International Journal of Stroke*, vol. 17, no. 1, pp. 18–29, 2022.

[2] C. P. Warlow *et al.*, *Stroke: practical management*. John Wiley & Sons, 2011.

[3] M.-C. Smith, W. D. Byblow, P. A. Barber, and C. M. Stinear, "Proportional recovery from lower limb motor impairment after stroke," *Stroke*, vol. 48, no. 5, pp. 1400–1403, 2017.

[4] Y. Fang and Z. F. Lerner, "Bilateral vs. Paretic-Limb-Only Ankle Exoskeleton Assistance for Improving Hemiparetic Gait: A Case Series," *IEEE Robot. Autom. Lett.*, vol. 7, no. 2, pp. 1246–1253, 2022.

[5] J. S. Lora-Millan, J. C. Moreno, and E. Rocon, "Assessment of gait symmetry, torque interaction and muscular response due to the unilateral assistance provided by an active knee orthosis in healthy subjects," *Proc. IEEE RAS EMBS Int. Conf. Biomed. Robot. Biomechatronics*, vol. 2020-Novem, no. 688175, pp. 229–234, 2020.

[6] H. Kawamoto *et al.*, "Development of an assist controller with robot suit HAL for hemiplegic patients using motion data on the unaffected side," *2014 36th Annu. Int. Conf. IEEE Eng. Med. Biol. Soc. EMBC 2014*, pp. 3077–3080, 2014.

[7] L. N. Awad, J. Bae, P. Kudzia, A. Long, T. Ellis, and C. J. Walsh, "Reducing circumduction and hip hiking during hemiparetic walking through targeted assistance of the paretic limb using a soft wearable robot," vol. 96, pp. 1–18, 2020.

[8] M. R. Tucker *et al.*, "Control Strategies for Active Lower Extremity Prosthetics and Orthotics : A Review," *J. Neuroeng. Rehabil.*, vol. 12, no. January 2015, 2015.

[9] T. Yan, M. Cempini, C. M. Oddo, and N. Vitiello, "Review of assistive strategies in powered lower-limb orthoses and exoskeletons," *Rob. Auton. Syst.*, vol. 64, pp. 120–136, 2015.

[10] R. Baud, A. R. Manzoori, A. Ijspeert, and M. Bouri, "Review of control strategies for lower-limb exoskeletons to assist gait," *J. Neuroeng. Rehabil.*, vol. 18, no. 1, p. 119, 2021.

[11] G. Cappellini, Y. P. Ivanenko, R. E. Poppele, and F. Lacquaniti, "Motor patterns in human walking and running," *J. Neurophysiol.*, vol. 95, no. 6, pp. 3426–3437, 2006.

[12] V. Ruiz Garate *et al.*, "Walking assistance using artificial primitives: A novel bioinspired framework using motor primitives for locomotion assistance through a wearable cooperative exoskeleton," *IEEE Robot. Autom. Mag.*, vol. 23, no. 1, pp. 83–95, 2016.

[13] P. F. Nunes, I. Ostan, and A. A. Siqueira, "Evaluation of motor primitive-based adaptive control for lower limb exoskeletons," *Frontiers in Robotics and AI*, vol. 7, p. 575217, 2020.

[14] T. Yan, A. Parri, V. Ruiz Garate, M. Cempini, R. Ronsse, and N. Vitiello, "An oscillator-based smooth real-time estimate of gait phase for wearable robotics," *Auton. Robots*, vol. 41, no. 3, pp. 759–774, 2017.

[15] H. Laloyaux and R. Ronsse, "Reconstruction of hip moments through constrained shape primitives," *Biosyst. Biorobotics*, vol. 27, pp. 383–388, 2022.

[16] H. Laloyaux *et al.*, "Experimental assessment of a control strategy for locomotion assistance relying on simplified motor primitives," in *2022 IEEE/RSJ International Conference on Intelligent Robots and Systems (IROS)*, 2022, pp. 12 254–12 260.

[17] S. J. Olney and C. L. Richards, "Hemiparetic gait following stroke. Part I : Characteristics," *Gait Posture*, vol. 4, no. 2, pp. 136–148, 1996.

[18] G. Van Der Velde, H. Laloyaux, and R. Ronsse, "Inducing asymmetric gait in healthy walkers: a review," 2023, under review.

[19] ——, "The effect of added ankle weight to gait in healthy subjects: a pilot study," Experimental data, Université catholique de Louvain, Tech. Rep., 2021.

[20] V. Ruiz Garate *et al.*, "Experimental validation of motor primitive-based control for leg exoskeletons during continuous multi-locomotion tasks," *Front. Neurorobot.*, vol. 11, p. 15, 2017.

[21] E. Martini *et al.*, "Gait training using a robotic hip exoskeleton improves metabolic gait efficiency in the elderly," *Sci. Rep.*, vol. 9, no. 1, pp. 1–12, 2019.

[22] A. Pergolini *et al.*, "Real-time locomotion recognition algorithm for an active pelvis orthosis to assist lower-limb amputees," *IEEE Robot. Autom. Lett.*, vol. 7, no. 3, pp. 7487–7494, 2022.

[23] F. Giovacchini *et al.*, "A light-weight active orthosis for hip movement assistance," *Rob. Auton. Syst.*, vol. 73, pp. 123–134, 2015.

[24] E. Martini *et al.*, "Pressure-sensitive insoles for real-time gait-related applications," *Sensors (Switzerland)*, vol. 20, no. 5, p. 1448, 2020.

[25] K. K. Patterson *et al.*, "Gait Asymmetry in Community-Ambulating Stroke Survivors," *Arch. Phys. Med. Rehabil.*, vol. 89, no. 2, pp. 304–310, 2008.

[26] B. L. Welch, "On the Comparison of Several Mean Values: An Alternative Approach," *Biometrika*, vol. 38, no. 3/4, p. 330, 1951.

[27] A. Trujillo-Ortiz. (2022) MATLAB Central File Exchange. Retrieved August 3, 2022. [Online]. Available: https://www.mathworks.com/matlabcentral/fileexchange/37123-welchanovawd

[28] S. J. Olney, M. P. Griffin, T. N. Monga, and I. D. McBride, "Work and power in gait of stroke patients," *Arch. Phys. Med. Rehabil.*, vol. 72, no. 5, pp. 309–314, 1991.

[29] Q. Zhang *et al.*, "Imposing Healthy Hip Motion Pattern and Range by Exoskeleton Control for Individualized Assistance," *IEEE Robot. Autom. Lett.*, vol. 7, no. 4, pp. 11 126–11 133, 2022.

[30] Y. Qian, H. Yu, and C. Fu, "Adaptive Oscillator-Based Assistive Torque Control for Gait Asymmetry Correction with a nSEA-Driven Hip Exoskeleton," *IEEE Trans. Neural Syst. Rehabil. Eng.*, vol. 30, pp. 2906–2915, 2022.

[31] D. S. Reisman, R. Wityk, K. Silver, and A. J. Bastian, "Split-belt treadmill adaptation transfers to overground walking in persons poststroke," *Neurorehabilitation and neural repair*, vol. 23, no. 7, pp. 735–744, 2009.

[32] K. Genthe, C. Schenck, S. Eicholtz, L. Zajac-Cox, S. Wolf, and T. M. Kesar, "Effects of real-time gait biofeedback on paretic propulsion and gait biomechanics in individuals post-stroke," *Topics in Stroke Rehabilitation*, vol. 25, no. 3, pp. 186–193, 2018.

[33] R. Ronsse, S. M. M. De Rossi, N. Vitiello, T. Lenzi, M. C. Carrozza, and A. J. Ijspeert, "Real-time estimate of velocity and acceleration of quasi-periodic signals using adaptive oscillators," *IEEE Trans. Robot.*, vol. 29, no. 3, pp. 783–791, 2013.